Polymer Chemistry

PAPER

View Article Online
View Journal | View Issue

Cite this: *Polym. Chem.*, 2018, **9**, 845

Multivalent polyrotaxane vectors as adaptive cargo complexes for gene therapy†

Rodinel Ardeleanu,[a] Andrei I. Dascalu,[a] Andrei Neamtu,[a,b] Dragos Peptanariu,[a] Cristina M. Uritu,[a] Stelian S. Maier,[a,c] Alina Nicolescu,[a] Bogdan C. Simionescu,[a,d] Mihail Barboiu[e] and Mariana Pinteala *[a]

This paper describes the philosophy to design, and a procedure to construct polyrotaxane-type gene carriers, together with the proof of their ability to conjunctively cooperate in order to generate cargo-complexes with dsDNA, able to efficiently transfect cultured cells. The main feature of these entities is their functionality as a cargo-complex that chemomimic the histones, and morphomimic the nucleosome. The polyrotaxane contains a PEG axle end-capped with silatrane cages, allowing the threading of nine cyclodextrin units, functionalized with polyethylenimines (PEI, 2 kDa). The obtained ROT-PEI multivalent architecture is similar to a giant PEI polycation, but devoid of the toxicity of large PEIs. To increase the cargo-complexes' versatility and to reduce their cytotoxicity, the study has been complemented with two other types of carriers: (i) including a mixture of PEI and short PEG molecules (ROT-PEI-PEG_{750}), and (ii) with PEI branches post-decorated with guanidine or arginine (ROT-PEI-G; ROT-PEI-Arg). The molecular geometry and the overall interactions of the synthesized carriers were investigated *in silico*. The experimental DNA binding capacity of these carriers in relationship with size, morphology and electrical charge was evaluated. The *in vitro* tests, showing the cytotoxicity and transfection efficiency of the investigated carriers, provided new information on gene vector design.

Received 26th July 2017,
Accepted 6th September 2017

DOI: 10.1039/c7py01256j

rsc.li/polymers

Introduction

According to the most recent global review,[1,2] until June 2012 the FDA approved 1843 clinical trials implying DNA and RNA vectorization for gene therapy purposes. Two-thirds of them have used viral vectors, despite their deficiencies like immunogenicity and low carrying capacity.

The need to increase the number of transferred nucleotides has promoted the use of non-viral vectors as reliable competitors. Their main advantage consists of the theoretical possibility to fully design them, and to accurately assemble them through chemical and physical–chemical approaches and techniques. However, the reduced transfer efficacy remains their significant drawback.

Cargo-complexes represent promising "tools" to deliver large amounts of sophisticated and/or sensitive pharmaco- and bio-active species.[3–5] In chemical terms, they are dynamic supramolecular bio-carrier conjugates. As functional aggregates, they exploit the particular reciprocal supramolecular affinity and dynamical steric complementarity between the carrier(s) and the active counterparts, to optimally transfer the genes, under "stealth" or at least under protected conditions, through biological media and barriers. Due to the fact that, usually, the molecules to be transported are functional entities *per se*, and it is mandatory to not alter them, the key components of the cargo-complexes are the carrier molecules. They must be chemically designed to show selective affinity toward the "cargo" molecules, and be endowed with molecular segments active against both the biological targets and the biochemical "assailants and hindrances". In the particular case of gene therapy (which makes use of DNA segments or plasmids, of integral RNA macromolecules, of ribozymes or of

[a]*Centre of Advanced Research in Bionanoconjugates and Biopolymers, "Petru Poni" Institute of Macromolecular Chemistry, 700487 Iasi, Romania. E-mail: pinteala@icmpp.ro*
[b]*Regional Institute of Oncology (IRO), TRANSCEND Research Center, 2-4 General Henry Mathias Berthlot Str., 700108 Iasi, Romania*
[c]*Department of Textile and Leather Chemical Engineering, "Gheorghe Asachi" Technical University of Iasi, 700050 Iasi, Romania*
[d]*Department of Natural and Synthetic Polymers, "Gheorghe Asachi" Technical University of Iasi, 700050 Iasi, Romania*
[e]*Adaptive Supramolecular Nanosystems Group, Institut Européen des Membranes, ENSCM/UMII/UMR-CNRS 5635, 34095 Montpellier, Cedex 5, France*

†Electronic supplementary information (ESI) available: Additional experimental data concerning synthesis of ROT precursor conjugates including NMR, FTIR spectra, a table resuming elemental analysis of the four polyrotaxane vectors, the GPC curve of ROT-PEI product in water, gel retardation assay results, the variation of zeta potential depending on N/P ratios of rotaxane based polyplexes, TEM images of polyplex particles and the corresponding size distribution, cytotoxicity and transfection efficiency results of the tested compounds. See DOI: 10.1039/c7py01256j

oligonucleotides to cure or to prevent the expression of maladies of genetic origin or with a genetic "echo"),[6–9] cargo-complexes play the major role of non-viral delivery systems, due to their ability to target specific cells (or cells passaging the cell-division cycle) and to inject their (macro)molecular "cargo" into them.

To transport large functional nucleic acids, the cooperation[10] of a variable but high number of polycationic carrier molecules is a must. Mainly as a consequence of the conformational flexibility of the carriers' edifice, the resulting supramolecular aggregates gain the advantage of tight complexation between the oppositely charged partners, which significantly reduces the volume of cargo-complexes and increases their transport and/or transfer efficacy.[11] To function in a reproducible manner, carriers must be themselves reproducibly produced. In this regard, the essential requirements consist of their detailed molecular design, and their accurate (even if complex) synthesis.

Research efforts are currently made to maintain the carriers as simple as possible, by "encumbering" them with the minimal amount of necessary molecular segments that confer them the required ternary functionality in relation to: (i) the nucleic acids to be transported, (ii) the external and/or nuclear membranes of the target cells to be penetrated, and (iii) the biologic/biochemical environment to accommodate oneself harmlessly (biomolecular and cell species, biochemical and biophysical mechanisms of living matter). Therefore, based on the chemical reasoning pathways, apparently "exotic" components were tested to build efficacious carriers. Particular and multi-functional cargo-complexes were developed to use them as platforms for vectorization.[12–15] The mechanisms they use to transport the nucleic acids are complex and conditionally reproducible (being usually limited to a restrained set of experimental parameters), thus preventing carrier "typification" and compelling the development of a broad variety of carrier architectures. A potential solution to unify the nucleic acid vectorization could be the addition of free branched polycationic molecules (non- or low-cytotoxic) which seems to increase the efficacy of barrier penetration,[16,17] *via* a fluctuant extra positive charge compensation, resulting from a local loose or bad packaging during DNA binding. This was the rationale behind the development of dynamically organized supramolecular carriers based on unimers assembling under the topo-chemical requests issued by sterically complex "cargoes". Recently, our group demonstrated the performances of carriers organized around fullerene and cyclic methylsiloxane as cores, equipped with shells that include a controllable number of cationic "arms" consisting of low molecular weight branched poly(ethylene imine) (PEI, 2 kDa).[10,18] We have also investigated the transfection ability of non-viral vectors produced by the techniques of constitutional dynamic chemistry (by dynamic constitutional framework chemistry).[19,20] Incentive results were obtained in both cases, but the versatility remained conditional.

In this work we report the philosophy to design, and a procedure to construct carriers of cyclodextrin-based polyrotaxane-type, and we prove their ability to conjunctively cooperate to generate cargo-complexes with plasmid DNA, able to efficiently transfect cells in culture. Polyrotaxanes are a variety of topological polymers which include "mechanically-linked" constituents in their structure. From the chemical point of view, they are supramolecular assemblies generated by the physical insertion of several macrocycles onto a linear (macro)molecule (generically named axle); since the resulting construct does not involve covalent links, to prevent the macrocycles slipping-off that would result in assembly unraveling, bulky molecules (named stoppers) are attached at both ends of the axle.[21] We obtained polyrotaxane carriers having an axle of precise length (consisting of a 1 kDa polyethylene glycol molecule, PEG_{1000}), which allow the threading of nine functionalized cyclodextrin units (CD), and end-capped with silatrane molecules (tricyclic cage-like heterocycles with a silicon heteroatom). The functional moiety is based on 2 kDa branched polyethyleneimine (PEI) molecules and thus the resulting highly flexible PEI-brush architecture could be seen as the equivalent of a giant PEI polycation with a molecular mass of 54 kDa, but devoid of the toxicity of large PEI molecules.

The key element of the functionality of a carrier consists of its ability to adapt to the molecular peculiarities of nucleic acids, particularly to their flexibility in confined spaces, based on which they can be packed in incredibly small volumes and regularly organized by means of histone proteins to generate the compact nucleic chromatin.[22] According to a biomimetic philosophy, we chemically designed the polyrotaxane-type carrier to acquire the functional characteristics of histone octameric complexes, but a quasi-linear structure which, together with the combined mobility of the CD units on the axle and of the engrafted PEI chains, allow the carrier to outwardly encompass nucleic acid molecules to form a wrapping/folding support and even to act as bridging entities between different segments of the polyanionic cargoes. Compact cargo-complexes of nanoparticulate shape result as a consequence.

Fig. 1 summarizes the structural and functional peculiarities of the polyrotaxane carriers we developed, and of the cargo-complexes they are able to construct with plasmid- or dsDNA.

To reduce the carrier cytotoxicity and to increase their physical–chemical versatility in loading nucleic acids, two supplemental ways to functionalize the CD units were investigated: (i) with a mixture of PEI and short linear poly(ethyleneglycol) molecules (PEG), and (ii) by post-decorating PEI branches with ionisable small molecules: guanidine and arginine. Both alternatives numerically diminish the positive charges supported by the carrier, the first of them to a greater extent, and thus both reduce the packaging capacity of the carriers. However, the subsequent advantage consists of the increase of spatial adaptability to the nucleic acids to be loaded and transported. The synthetic pathways for the intermediate compounds, together with their characteristics, are described in the ESI.†

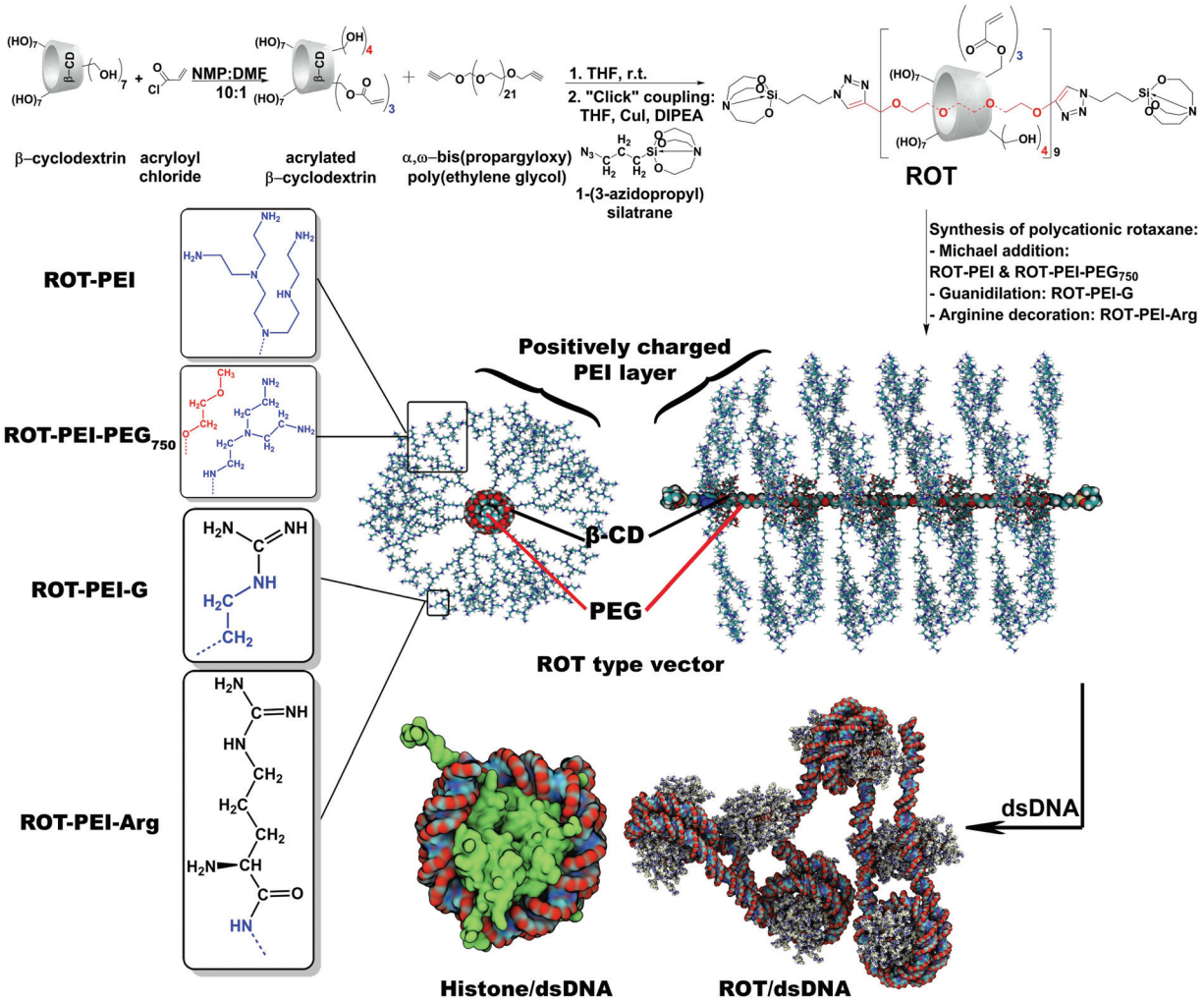

Fig. 1 Synthesis of ROT-PEI, ROT-PEI-PEG_{750}, ROT-PEI-G, ROT-PEI-Arg polyrotaxane carriers, and the structure of the postulated nucleosome-like cargo-complexes they generate by complexation with dsDNA. The histone/dsDNA coordinates were taken from the literature.[23]

Results and discussion

On the rationale of the design of polyrotaxane carrier

Because of their reproducible and controllable reactivity, cyclodextrins were frequently used as cores or as connectors for building carrier molecules.[24–29] Their propensity to thread on linear molecular segments[30] recommends cyclodextrins for the building of mechanically interlocked supramolecular structures of (poly)rotaxane type[31–34] which potentially act as nucleic acid carriers.[35–40]

The chemical design of polyrotaxanes is approached considering their final applications,[41] and the synthesis is performed according to sophisticated strategies[42] which usually make use of enthalpic driving forces to induce the precursors' self-assembly.[43] As an example, hydrophilic–hydrophobic interactions (solvophilicity) are first exploited to generate a pseudo-polyrotaxane,[44] then the stoppers are covalently attached to "lock" the structure.

Functionalized-cyclodextrin-based polyrotaxanes are largely tested as carriers.[45–48] They valorize the flexibility of the axle, the diversity of the lateral chains grafted on cyclodextrin units, and the ability to control the number of threaded macrocycles. The last mentioned parameter (also known as "the linear density of threaded cyclodextrin molecules", or "the treading ratio") is the most important when the complexation capacity of carriers (and therefore the vectorization efficacy of cargo-complexes) must be large. In theory, if the axle consists of a chain of poly(ethylene glycol), cyclodextrins (having a "thickness" of 0.79 nm) could be inserted along at a maximum density of one molecule for each two and a half repeating units ($-CH_2-CH_2-O-$, of 0.34 nm length),[49–52] but the threading ratio can be controlled if more complex axle macromolecules are used.[53,54]

Usually, cyclodextrin-based polyrotaxanes are synthesized by solvophobically driven templation,[55] a method of statistical threading. If rigorous molecular edifices must be obtained, a

technique of step-growth polymerization of pseudorotaxanes (complexes that lack stoppers) may be applied.[56,57]

Polyrotaxanes that include cationic derivatized cyclodextrin molecules are particularly used as carriers for nucleic acids.[45,58–61] Their *complexation efficacy* and *intracellular fate* are the parameters which can be decided by chemical design.[62,63] The first one mainly depends on the cationic charge density, length, flexibility, branching amplitude and the number of molecules grafted on the macrocycles, and on the number of derivatized cyclodextrin molecules inserted onto the axle. The second one can be controlled by preferentially selecting biocleavable polyrotaxanes as carriers.[64] Biocleavability (and particularly, cytocleavability) is a key feature for the success of all delivery techniques, especially for the intracellular ones. It involves the indiscriminatory biochemical breaking of some molecular segments of the carrier (for example by the reductant activity of the cytosol or of nuclei),[65] or the rigorous enzyme-mediated selective disjunction of the carrier components. The second mentioned mechanism of biocleavage allows a precise intracellular targeting, and implicitly the treatment of particular diseases.[66] The biocleavability could be induced by selecting the molecular type of the rotaxane axle and/or stoppers, or by the insertion of particular chemical bonds as connection locks between the polyrotaxane components (especially between the axle and stopper molecules). Disulfide covalent linkage and terminal-peptide groups are frequently used.[67–69]

We selected a silatrane molecule to end-cap the polyrotaxane. Silatranes are organosilicon tricyclic compounds, relatively rigid and bulky.[70,71] Due to the penta-coordinated silicon atom, silatranes are hydrolytically labile compounds that decompose according to the first-order kinetics in acidic milieus, but are fairly stable under reductive conditions at neutral pH.[72,73]

Chemical syntheses and characterization of polyrotaxane carriers

Generically, the synthesis of polyrotaxane carriers supposes four steps: (i) CD activation by the esterification of some of the OH-6 primary hydroxyl groups with acryloyl chloride, concluded with the insertion of unsaturated molecule segments which can be involved in further addition reactions, (ii) the synthesis of a poly(pseudorotaxane) by inserting activated CD molecules onto the axle consisting of activated 1 kDa PEG molecules [α,ω-bis-(propargyloxy)-PEG_{1000}], (iii) the capping of the poly(pseudorotaxane) by the reaction with activated silatrane molecules, to obtain the "raw" polyrotaxane, and (iv) the functionalization of the polyrotaxane pertaining activated CDs by the addition of primary amine-containing molecules (branched PEI and, possibly, methoxypolyethylene glycol amine). A fifth supplemental step might be completed in order to post-functionalize the cationic PEI branches, by decorating them with guanidine or arginine moieties.

The synthesis of α,ω-bis-{1-[3-(silatranyl)prop-1-yl]-1*H*-1,2,3-triazol-5-yl}-PEG_{1000}/acrylated β-CD polyrotaxane (ROT), corresponding to step (iii) of the above-mentioned series, took place according to the scheme presented in Fig. 2. The precursors of β-CD poly(pseudorotaxane) and 1-(3-azidopropyl)silatrane have been synthesized and fully characterized following the procedures presented in the ESI.† As proven by ^{1}H-NMR spectroscopy, the β-CD poly(pseudorotaxane) contains 9 acrylated β-cyclodextrin units on the PEG axle.

The formation of silatrane-triazole-propyl units is indicated in the ^{1}H-NMR spectrum (Fig. S22†) by the appearance of the following characteristic signals: 0.16 ppm, a broad signal assigned to the propyl CH_2 groups linked directly to the silicon atoms; 1.67–1.96 ppm, a multiplet assigned to the CH_2–CH_2–Si groups from the propyl chain; 2.80 ppm, a triplet assigned to the silatrane CH_2 groups linked to the nitrogen atoms; 3.61 ppm, a triplet assigned to the silatrane CH_2 groups linked to the oxygen atoms, and 8.37 ppm, a broad signal assigned to the CH groups from the triazole unit. The disappearance of the two signals characteristic of the propargyl units, the triplet from 3.43 ppm (CH groups) and the doublet from 4.15 ppm (CH_2 groups), while the PEG signal at 3.52 ppm is still present in the ^{1}H-NMR spectrum, are other indications for the formation of the desired silatrane-triazole-propyl end groups.

The FT-IR spectrum (Fig. S23†) of α,ω-bis-{1-[3-(silatranyl) prop-1-yl]-1*H*-1,2,3-triazol-5-yl}-PEG_{1000}/acrylated β-CD polyrotaxane is similar to that of the poly(pseudorotaxane) revealing the absorption bands specific to hydroxyl groups at 3477 cm^{-1}, methylene groups at 2927 cm^{-1} and carbonyl groups C═O at 1733 cm^{-1}. The absence of the absorption band at 2100 cm^{-1} indicated the conversion of the azide group to a triazole cycle.

The XRD results are depicted in Fig. 3 and are in agreement with previously reported data.[74,75] Simultaneously large peaks at 2θ angles of 10.5° (typical for the modified β-CD/polymer crystallites), 18.5° and 23.3° (typical for PEO crystallites) confirm the formation of the rotaxane structure. In addition, the X-ray diffractogram of ROT presents a small wide peak at less than $2\theta = 10°$ (typical for modified β-CD), attributed to the supramolecular aggregation which occurred.

The synthesis of the vector based on the polyrotaxane decorated with PEI (ROT-PEI) was performed according to the reaction scheme presented in Fig. S24.†

The ^{1}H-NMR spectrum of the polyrotaxane-type carrier is dominated by the signals from PEI and PEG components, and almost all of them appear in the 2.5–4 ppm interval, as presented in Fig. S25.† The success of the coupling reactions is indicated by the disappearance of the acryloyl group signals from the 5.79–6.40 ppm region. The PEI component has a characteristic "fingerprint", with all the signals overlapping in the 2.1–3.5 ppm interval. The PEG component has a characteristic sharp singlet at 3.71 ppm, assigned to the methylene protons from the main chain. Most of the signals corresponding to β-CD are overlapped by the PEG signals (3.55–4.00 ppm) and could not be identified. The broad signal at 5.08 ppm corresponds to the β-CD protons in position 1. Other characteristic signals which could be identified in the ^{1}H-NMR spectrum are the broad signal at 0.64 ppm, assigned to the propyl CH_2 groups directly linked to the silicon atoms, and the broad signal at 8.07 ppm assigned to the CH groups from the triazole unit. The solvent for the

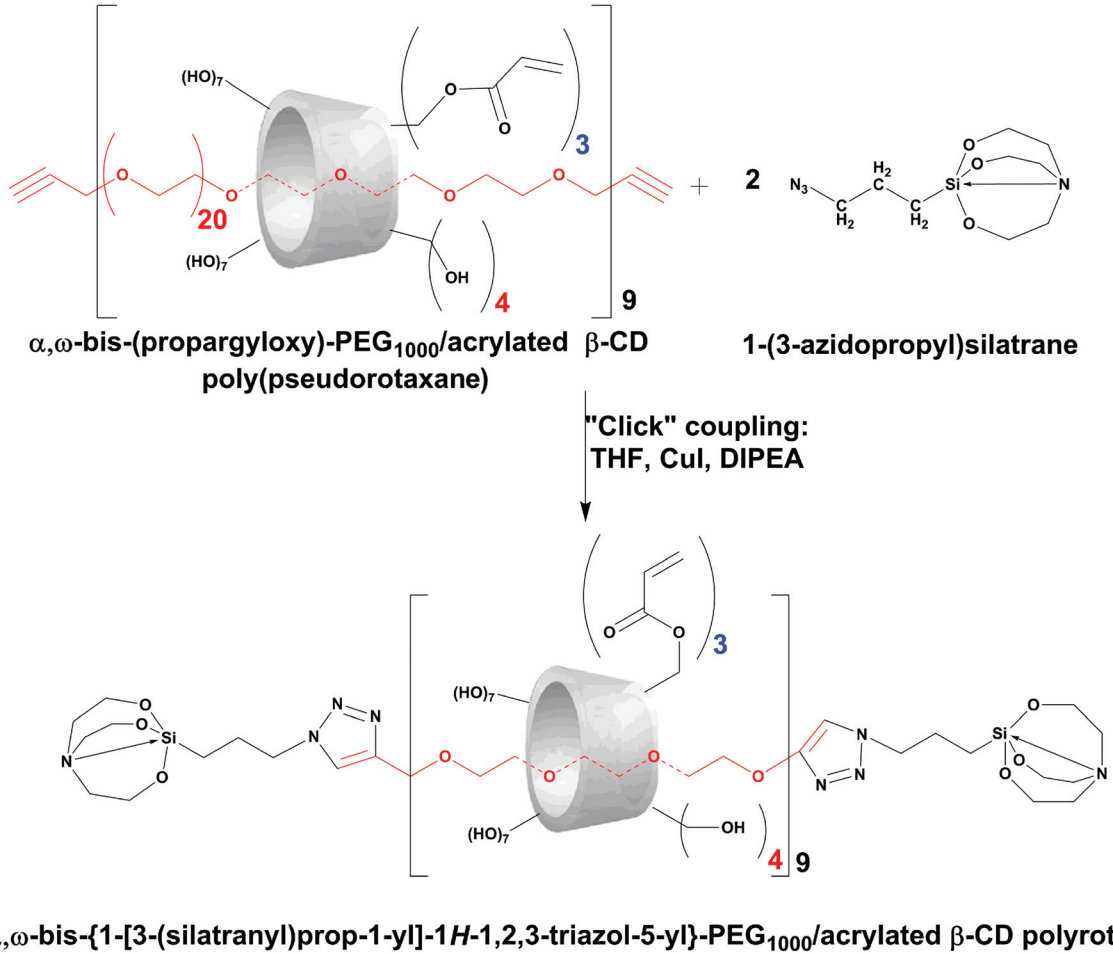

Fig. 2 Schematic representation of α,ω-bis-{1-[3-(silatranyl)prop-1-yl]-1*H*-1,2,3-triazol-5-yl}-PEG_{1000}/acrylated β-CD polyrotaxane synthesis procedure.

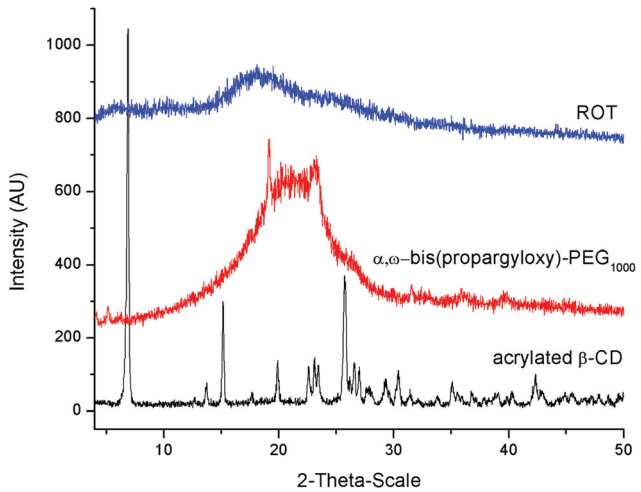

Fig. 3 XRD results of ROT, α,ω-bis(propargyloxy)-PEG_{1000} and acrylated β-CD.

NMR analysis being D_2O, the protons from hydroxyl and amine groups no longer appear in the spectrum, being exchanged with deuterium.

Fig. S26† depicts the results of the gel permeation chromatography assay applied to the synthesized ROT-PEI product. The M_n value, of 64 438 g mol^{-1}, confirms the expected value of molecular weight.

The synthesis of the vector based on the polyrotaxane decorated with PEI and short linear poly(ethylene glycol) (PEG_{750}) (ROT-PEI-PEG_{750}) was conducted as described in the Experimental section and is summarized in Fig. S27.†

The ^{1}H-NMR spectrum of ROT-PEI-PEG_{750} is almost identical to that of the ROT-PEI derivative, as given in Fig. S28.† From the ^{1}H-NMR point of view, no significant difference between the two types of PEG moieties attached to the ROT structure is observed. However, in the ^{1}H-NMR spectrum of ROT-PEI-PEG_{750} rotaxane, one can observe an intensity increase of the singlet at 3.71 ppm, previously assigned to the PEG's methylene protons from the rotaxane axle. This indicates an increase in methylene proton concentration, caused by the addition of PEG_{750} moieties to the acrylic groups. The appearance in the ^{1}H-NMR spectrum of ROT-PEI-PEG_{750} rotaxane of the singlet from 3.37 ppm, assigned to the PEG_{750}'s methoxy end groups (see Fig. S28-B†), is another indication of the addition of the PEG_{750} moieties.

The vibration band of the valence vinyl –CH=CH_2 group (acryloyl residues) at 1413 cm^{-1} in the FT-IR spectra of the branched polyethyleneimine decorated polyrotaxane disappeared as a direct consequence of the addition of amino groups in the PEI segments to the double bonds, while a new absorption band appeared at 1471 cm^{-1} due to their conversion to ethylene groups (Fig. S29†).

The synthesis of ROT-PEI-Arg has been achieved by attaching arginine residues on the superficial amino groups of the branched polyethyleneimine in the ROT-PEI (Fig. S30†). The reaction has been conducted using a previously reported protocol.[76,77]

The ^{1}H-NMR spectrum of ROT-PEI-Arg (Fig. S31†) is very similar to that of the parent rotaxane ROT-PEI, being dominated by the signals from the PEI component. The arginine moieties have characteristic signals in the following spectral regions: 1.60–1.80 ppm – two multiplet type signals from the methylene groups in positions 3 and 4, a triplet centered at 3.22 ppm from the methylene group in position 5 and another triplet centered at 3.52 ppm from the methylene group in position 2. These last two signals are partially overlapped by the signals characteristic of PEI moieties.

ROT-PEI-G has been obtained by grafting guanidine on the superficial primary amino groups of ROT-PEI. The molar ratio between the two reaction components was 1 : 27 ROT-PEI : 1*H*-pyrazole-1-carboxamidine hydrochloride, in order to attach a guanidine addend to a single amino group in each branched PEI in the polyrotaxane structure.

To investigate the chemical structure of ROT-PEI-G the bidimensional ^{1}H,^{13}C-HMBC spectrum (Fig. S32†) was necessary since the ^{1}H-NMR spectrum of ROT-PEI-G is almost identical to that of ROT-PEI, as the guanidine moiety has no protonated carbon atoms. Since the sample was analyzed in D_2O, all signals corresponding to protonated nitrogen or oxygen atoms no longer appear in the spectrum due to the exchange of these labile protons with deuterium atoms. In the ^{1}H,^{13}C-HMBC spectrum, the appearance of cross peaks between carbons from 158–160 ppm and protons from 3.0–3.5 ppm was observed, indicating the couplings over 3 bonds of the carbon atom from guanidine with the methylene protons from the PEI moiety. Moreover, they cannot be confused with the correlation peaks between esteric carboxyl groups of acrylated β-cyclodextrin units and methylene protons resulting from the addition of PEI to acrylic groups of β-CD at 165–173 ppm in the ^{13}C-NMR spectrum. These correlation peaks were not present in the ^{1}H,^{13}C-HMBC spectrum recorded for ROT-PEI (spectrum not shown).

The mass percent concentrations of the elements which have been found in the four studied carriers are given in Table S1.† The percentage values of nitrogen content were used to calculate the mixing ratio between carriers and nucleic acids, further expressed as N/P ratios.

On the rationale of *in silico* chemical modeling

Building atomistic models for the polyrotaxane aggregate has a particular importance as it can provide information on the dimensions of the aggregate at the atomic scale, as well as on the PEI layer structuring and its interaction with ions in solution. A model of the polyrotaxane was constructed based on the experimental ratios between different components, and further subjected to molecular dynamics simulations in explicit water/ion solvent. Initially, the aggregate was built by using separately constructed PEI and β-CD, which were then combined in an interlocked architecture on the PEG/stopper axle (Fig. 4). However, the generated model has an artificial conformation which does not reflect the true conformation adopted by the aggregate in solution. Thus, the model was subjected to molecular dynamics simulations to relax it towards a more characteristic shape in solution. Special attention was required for structure equilibration, using gradually relaxing atom positional restraints, as it was observed that cyclodextrin molecules were removed from the PEG/stopper if only energy minimization was employed prior to production run initiation.

To monitor the conformational relaxation and system equilibration during the production simulation (10 ns), the moments of inertia (MOI) around the principal axes were used as a measure of the structural deviation and plotted against the simulation time (Fig. S33-A†). MOIs were preferred over the more traditional root mean squared deviation (RMSD) of atomic positions due to the fact that PEI substituted cyclodextrins may rotate around the central PEG axis, giving thus falsely high RMSD values for a globally conserved polyrotaxane shape. It can be seen that the curve for the I_z moment, corresponding to the rotation around the principal axis aligned with the PEG backbone, initially decreased and then flattened after around 2.5 ns of simulation time. Thus, during the first 2.5 ns the PEI layer progressively relaxed from a more radially extended to a more collapsed conformation with respect to the central axis (PEG backbone) of the aggregate. The I_x and I_y moments, which correspond to rotation around the two principal axes perpendicular to the PEG backbone, remained largely constant as the PEI expansion along this direction was not so large.

The equilibrated structure after 10 ns of MD simulation displayed a rod-like shape with the PEI layer covering the PEG axle threaded through the β-CD macrocycles (Fig. S33-B†). This shape was stable throughout the last 7.5 ns and no detachment of β-CD from the PEG axle was observed. In the longitudinal direction the aggregate had a dimension of 12.61 nm, measured as the average distance between the most distant tertiary nitrogen atoms of PEI at the ends of the rotaxane axle. In the transversal plane the mean diameter was 5.36 nm (the average distance between the most distant tertiary nitrogen atoms of PEI belonging to the same β-CD). The distances were averaged over the last 7.5 ns of the production simulation, during which the aggregate could be considered fully equilibrated. Interestingly, the mean external transversal diameter of the positively charged PEI layer correlates very well with the diameter of the histone core of the nucleosome (~6.5 nm), the natural DNA packaging unit of chromatin in eukaryotic cells.

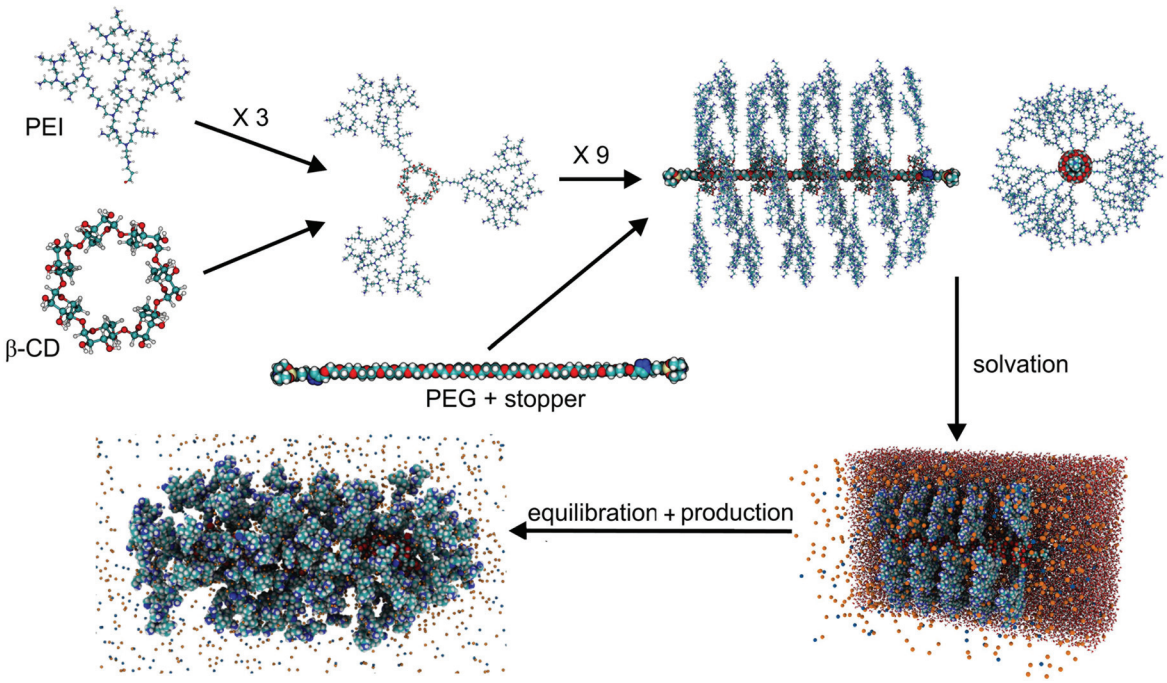

Fig. 4 The initial conformation taken into consideration for the polyrotaxane-type carrier, *in vacuo* (top), and in water/ion cage (bottom).

The molecular geometry and the overall reactivity of the ROT-PEI polyrotaxane-type carrier were investigated *in silico* by molecular dynamics simulation (described in the ESI†). Fig. 5 presents the results obtained using the Avogadro software application.

As revealed by the *in silico* study, in aqueous solution the synthesized ROT-PEI-PEG_{750} carrier should behave as a flexible nanorod (see Fig. 5(A)), about 12.6 nm long and 6.4 nm across, which sterically exposes positively charged branches (according to Fig. 5(B), these ones efficiently exclude Na^+ cations). Interestingly, the mean external transversal diameter of the positively charged PEI layer correlates very well with the diameter of the histone core of the nucleosome (~6.5 nm).[23]

To get insights into the distribution of water and ions around the polyrotaxane structure, bi-dimensional number density charts were computed in the plane perpendicular to the long axis of the aggregate, for different components. The averaged charts over the simulation time and over the longitudinal positions are depicted in Fig. 5(B) for PEI, water, and Cl^- and Na^+ ions respectively. The initially randomly distributed negative Cl^- ions became readily absorbed into the positively charged PEI layer, while Na^+ ions were largely excluded from the interior of the aggregate. Distribution of both negative and positive ions inside and at the surface of the PEI layer may play an important role in DNA complexation due to the competition arising between these ions on the one hand and the negatively charged DNA phosphate groups/positive PEI on the other hand. Water density is also lowered in the PEI region due to excluded volume interactions, which may give rise to osmotic induced longitudinal stress on the PEI "brush" layer and thus on the stability of the aggregate.

In silico estimation of the volume of cargo-complexes

In the particular case of the ROT-PEI carrier, the molecular volume, V_{Rot}, was calculated as being enclosed by the molecular surface constructed using YASARA, giving a result of 68.35 nm^3. Fig. S40-A† depicts the *in silico* results. To estimate the plasmid volume, a double length Dickerson–Drew DNA dodecamer 2 × d[CGCGAATTCGCG]$_2$ double helix chain was constructed and its volume was computed as above. Starting from this value, the volume of a single base pair was deduced as being 0.4703 nm^3. By multiplying with the plasmid base pair content (5991 bp), the total plasmid volume V_P was theoretically calculated, giving (0.4703 × 5991) 2817.57 nm^3 (see Fig. S40-B† for the 3D conformation). Furthermore, from the N/P ratio one could calculate the number of individual carriers complexing a single plasmid, which allows us to estimate the volume of the unit ROT-PEI-based cargo-complex. Two preliminary calculations must be done. First, considering the molecular mass of the ROT-PEI carrier (64 390 Da) and its nitrogen content (28.35%), the resulting number of nitrogen moles per carrier is calculated as being 1303. Second, each nucleobase includes one mole of phosphorous, thus the 5991 bp pCS2 + MT-Luc plasmid will contain 11 982 moles of phosphorous.

Therefore, at the best complexing N/P ratio of 20, the number of nitrogen moles involved in building one cargo-complex entity is (11 982 × 20) 234 640. As a consequence, the

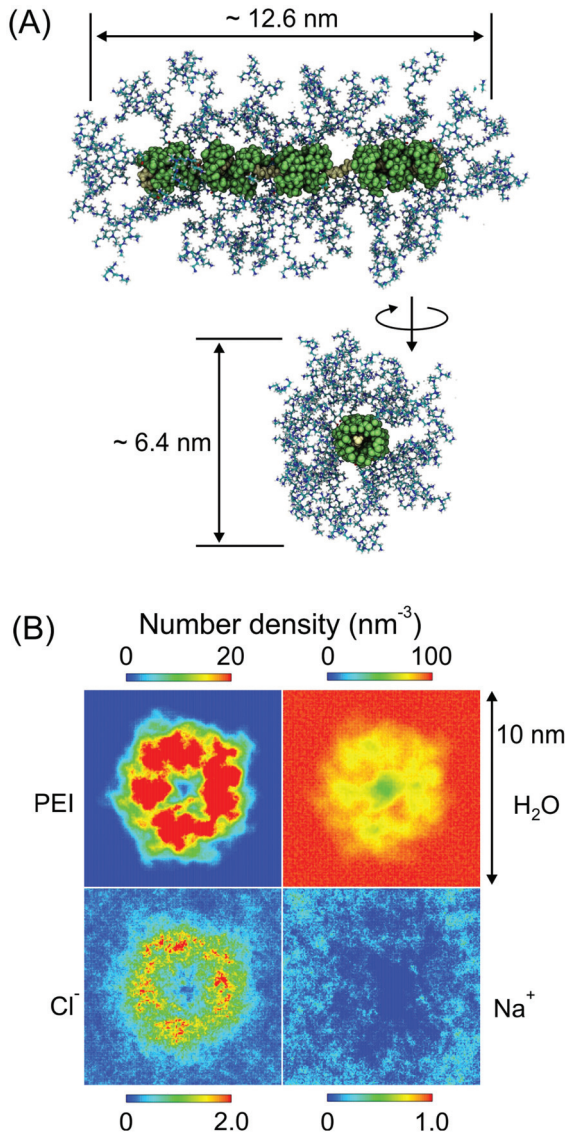

Fig. 5 The molecular geometry and the interaction of the ROT-PEI-PEG_{750} carrier with small chemical species. (A) The calculated dimensions of the nano-rod-like carrier molecule. (B) Bi-dimensional distribution charts (number of particles per volume) for the four most important components of the polyrotaxane carrier. The color scale of the plots is not identical due to the large differences in the concentration of the distinctive components.

number of carrier molecules contained in a cargo-complex is, on average, 180 (234 640/1303). Accepting that the volume of the cargo-complex entity represents the sum of its components' volume (one plasmid and 180 carrier molecules), the theoretical volume of an entity will be ($V_P + 180V_{Rot} = 2817.57 + 180 \times 68.35$) 15 120.27 nm^3. Accordingly, considering cargo-complexes as being spherical, their equivalent diameter should be about 31 nm. The fact that the TEM measured diameter of ROT-PEI-plasmid particles is about 110 nm, results in each of them accommodating a minimum of three and a maximum of 21 fully compacted individual ROT-PEI cargo-complexes (values calculated according to Gensane, T. (2003)[78]).

Binding affinity of carrier molecules and transfection ability of cargo-complexes

The experimental evaluation of the real binding affinity/capacity of an individual carrier molecule with respect to nucleic acids is difficult and doubtful. This is why a global efficacy is determined and expressed as the value of the carrier to dsDNA ratio starting with which a precisely measured quantity of nucleic acid is entirely and fully associated with a precisely weighed amount of carrier. The ratio is calculated considering the precise content of nitrogen in the carrier and of phosphorous in the nucleic acid, the so-called N/P value, that completely neutralizes (and thus prevents the electrophoretic migration of) the nucleic acid from its mixture with the carrier. The gel retardation assay (Fig. S34†) summarizes the packing ability of the four synthesized polyrotaxane carriers. The binding capacity of the investigated carriers decreases in the order of ROT-PEI (N/P > 15), ROT-PEI-G (N/P > 20), ROT-PEI-PEG_{750} (N/P > 30) and ROT-PEI-Arg (N/P > 40).

The zeta potential starts in all cases with negative values, corresponding to N/P of 1, and arises to the field of positive values increasing the N/P ratio (Fig. S37†). The minimum zeta potential of about −29 mV has been encountered in ROT-PEI-PEG_{750}/pDNA polyplex solution, at N/P 1. At the same N/P ratio, the other carriers displayed zeta potential values around −11 mV. The curves traced according to the evolution of zeta potential as a function of the N/P ratio show an ascending trend, becoming almost constant at large N/P ratios. The highest zeta potential values have been met for ROT-PEI (from −10.93 to 16.63 mV), followed by ROT-PEI-G (from −11.31 to 14.22 mV) and ROT-PEI-Arg (from −11.47 to 11.32 mV). An unexpected behavior has been observed for ROT-PEI-PEG_{750}, with a maximum zeta potential of 4.55 mV obtained at N/P 50. This very low value can be explained by the presence of PEG chains surrounding the conjugate macromolecule, which have in this case a masking effect of the positive charge normally existent in polycations. This deviation has not been shown to prevent the DNA binding ability (see gel retardation assay results) and even transfection efficiency.

We measured the transfection efficiency of the synthesized polyplexes by assaying the uptake of pLuc or pGFP plasmids by HeLa cells, after its complexation with the four carriers, and with 2 and 25 kDa PEI. The results are given in Fig. 7 as relative light units (RLUs) per 10 000 seeded cells. The ROT-PEI polyplexes exhibit the highest transfection efficiency, with a maximum yield at N/P 20, very similar to 25 kDa PEI whose drawbacks are well known. ROT-PEI-G also offers a very good transfection efficacy, with a maximum yield at N/P 30. ROT-PEI-Arg and ROT-PEI-PEG_{750}, having a maximum yield at N/P ratios of 60 and 70, respectively, exhibit lower transfection ability, which is however two or three times higher when compared to 2 kDa PEI. It is obvious that ROT-PEI-PEG_{750} and ROT-PEI-Arg have the ability to transfect in a wide range of the N/P ratio, from 30 to 80, unlike ROT-PEI and ROT-PEI-G which can transfect for N/P ratios from 5 to 30, and from 15 to 50, respectively.

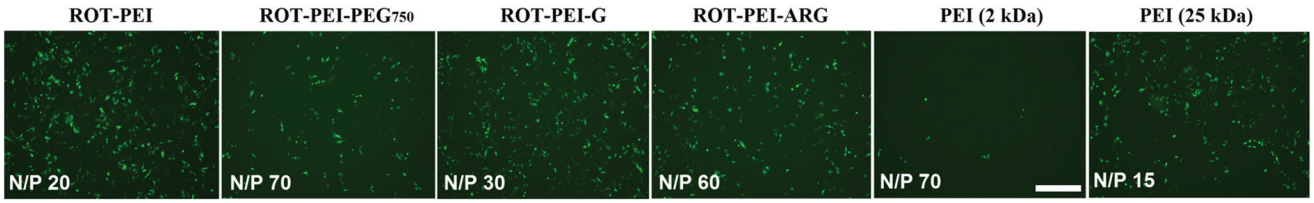

Fig. 6 Fluorescence microscopy images of transfected HeLa cells, using ROT-PEI/pGFP, ROT-PEI-PEG_{750}/pGFP, ROT-PEI-G/pGFP, ROT-PEI-Arg/pGFP and PEI (2 and 25 kDa)/pGFP cargo-complexes, at their particular optimal N/P ratios.

To better highlight the transfection process using these systems, pGFP-transfected cells were also subjected to a qualitative analysis by fluorescence microscopy (Fig. 6 and Fig. S36†). Similar predictable transfection efficiency was indicated by the maximum zeta potential values of polyplexes for different N/P ratios (ROT-PEI: 16.63 mV; ROT-PEI-G: 14.22 mV; ROT-PEI-Arg: 11.32 mV; ROT-PEI-PEG_{750}: 4.55 mV; Fig. S37†).

Fig. 7 presents the transfection ability of cargo-complexes generated between the pCS2 + MT-Luc plasmid and the four types of rotaxane carriers at different N/P ratios, using HeLa cells.

The collaborative packaging ability of the four types of carriers was experimentally proved by measuring the dimensions of the particulate cargo-complexes generated with the pCS2 + MT-Luc reporter plasmid (5991 bp). Fig. 8 includes the TEM images of the cargo-complexes obtained using the four types of polyrotaxane carriers, when the optimal N/P ratios were applied in order to attain the maximum transfection efficacy (which slightly differs from the ratios of maximal binding capacity). It should be pointed out that the dimensions of cargo-complexes generated between the pCS2 + MT-Luc plasmid and the four types of rotaxane carriers (ROT-PEI, ROT-PEI-PEG_{750}, ROT-PEI-G and ROT-PEI-Arg), at N/P ratios of maximum transfection, obtained by the dynamic light scattering (DLS) analysis (Table S2†) are slightly larger in comparison with those observed by TEM. The explanation resides in the fact that, during the preparation of TEM samples, the slow evaporation of the solvent concludes with a supplemental contraction of the initially swollen particles.[74,75]

Based on the TEM measured dimensions of the roughly spherical cargo-complex particles, one can calculate the approximate number of individual plasmids and carrier molecules which collaboratively bind a plasmid. As an example, in the case of the ROT-PEI carrier, the molecular volume, V_{Rot}, was calculated as being enclosed by the molecular surface constructed using the YASARA software, giving a result of 68.35 nm^3. Similar calculations indicate that the volume of the pCS2 + MT-Luc plasmid is 2817.57 nm^3. At the optimal N/P ratio, the minimal theoretical number of carrier molecules required to neutralize the negative charges of an intact plasmid is, on average, 180. As a consequence, the minimal volume of a cargo-complex containing one plasmid molecule will be 15 120.27 nm^3. Considering cargo-complexes as being spherical, their equivalent diameter should be about 31 nm. If the mean measured diameter of a particle comprising ROT-PEI-plasmid is 110 nm (equivalent to a volume of 696 910 nm^3), each of them should accommodate at least 3 lax assembled, but maximum 21 fully compacted, individual cargo-complexes.

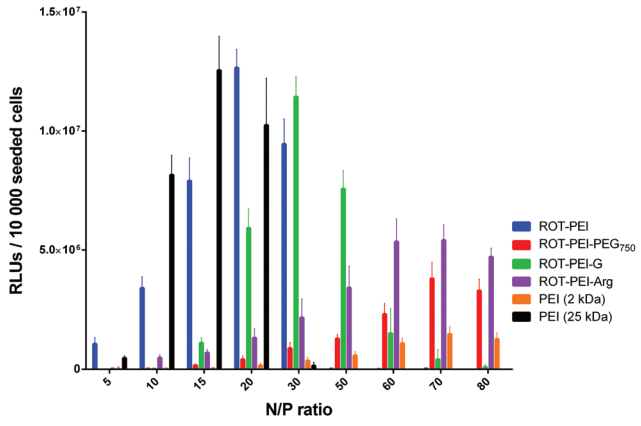

Fig. 7 The transfection efficiency results given by ROT-PEI, ROT-PEI-PEG_{750}, ROT-PEI-G, ROT-PEI-Arg, PEI 2 kDa, and PEI 25 kDa, with pCS2 + MT-Luc plasmid on HeLa cells, at all tested N/P ratios (from 5 to 80).

Conclusions

This paper reports the design, the synthesis and the characteristics of a new class of polyrotaxane carriers able to collaboratively generate cargo-complexes with nucleic acids. We have demonstrated the cargo-complexes' ability to transfect HeLa cells with a high efficiency. The individual carrier molecules consist of mechanically interlocked supramolecular assemblies comprised of a flexible 1 kDa PEG axle, capped with silatrane structures to withhold nine functionalized mobile cyclodextrin units. Due to the precise synthesis pathway, highly reproducible carriers are obtained. Exactly three units of pendant polycationic branches were grafted on each cyclodextrin unit in order to endow them with the ability to electrostatically interact with polyanionic nucleic acids. The efficacy and versatility of carrier molecules can be tailored through the functionality of the branches. Four types of such branches were tested to demonstrate that the ROT-PEI vehicle provides optimal transfection when plasmid dsDNA is to be transported into HeLa cells.

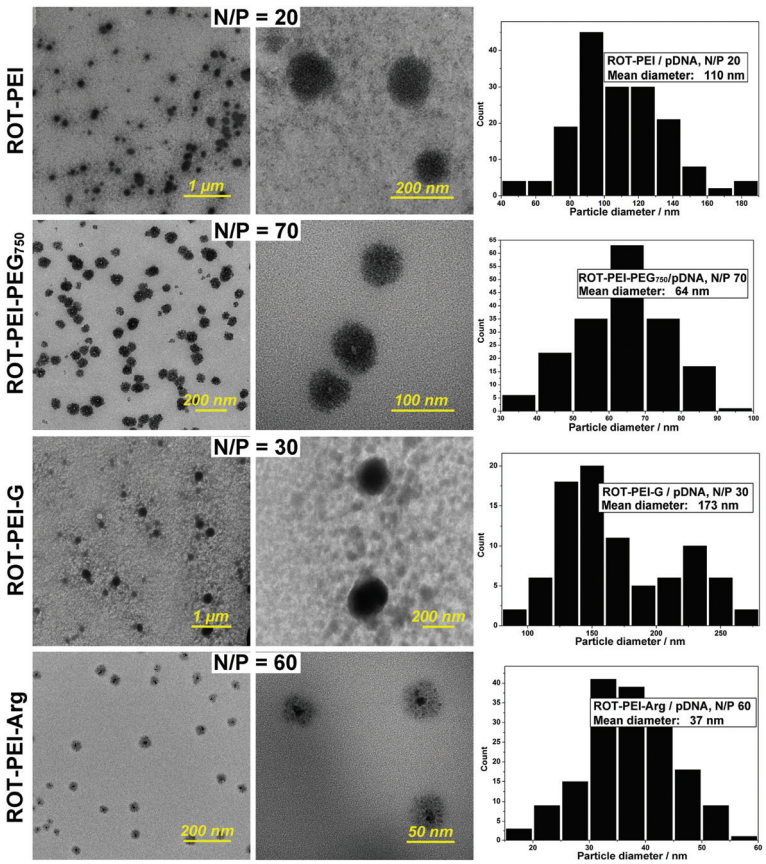

Fig. 8 TEM images of the cargo-complexes generated between the pCS2 + MT-Luc plasmid and the four types of rotaxane carriers.

Experimental section

Materials

Acryloyl chloride, 1-(3-bromopropyl)-trimethoxysilane, potassium hydroxide (KOH), triethanolamine, sodium hydride (NaH), poly(ethylene glycol) with average molecular weight of 1 kDa (PEG_{1000}), branched polyethylenimine (PEI) with average molecular weight of 2 kDa, methoxypoly(ethylene glycol)-amine hydrochloride with average molecular weight of 750 Da (PEG_{750}), propargyl bromide, sodium azide, anhydrous magnesium sulphate, cuprous iodide (CuI), silica gel 200–400 mesh 60 Å, molecular sieves UOP type 3 Å, 1*H*-pyrazole-1-carboxamidine hydrochloride, diisopropylethylamine (DIPEA), N^{α}-Fmoc-N^{ω}-(2,2,4,6,7-pentamethyldihydrobenzofuran-5-sulfonyl)-L-arginine (Fmoc-Arg(pbf)-OH), 1-hydroxybenzotriazole hydrate (HOBt), *N*,*N*,*N*′,*N*′-tetramethyl-*O*-(1*H*-benzotriazol-1-yl)uronium hexafluorophosphate (HBTU), trifluoroacetic acid (TFA), piperidine, triisopropylsilane (TIPS), methanol (abs.), acetone, tetrahydrofuran (THF), toluene, dimethyl sulfoxide (DMSO), *N*-methyl-2-pyrrolidone (NMP), *n*-hexane, chloroform, and methylene chloride were purchased from Sigma-Aldrich and used as received. SnakeSkin™ Dialysis Tubing, 3.5k MWCO, 22 mm was purchased from ThermoFischer Scientific. β-Cyclodextrin (β-CD) 97% was purchased from Sigma-Aldrich and dried using an Abderhalden's drying pistol for 48 h at 110 °C and 20 mbar. *N*,*N*-Dimethylformamide (DMF) purchased from Sigma-Aldrich was distilled over potassium hydroxide and stored over 3 Å molecular sieves. Plasmids pCS2 + MT-Luc (pLUC) and pCS2 + NLS-eGFP (pGFP) were a gift from Dr Adrian Salic, Harvard University, Boston.

Methods

Chemical syntheses. The synthesis and characterization of intermediate compounds are described in the ESI.†

Preparation of α,ω-bis-{1-[3-(silatranyl)prop-1-yl]-1*H*-1,2,3-triazol-5-yl}-PEG_{1000}/acrylated β-CD polyrotaxane (ROT). Initially, a CuACC catalyst solution was prepared by dissolving CuI (0.02 g, 0.2 mmol) and DIPEA (0.13 g, 1.0 mmol) in anhydrous degassed THF (3 mL) (Fig. S21†). Another solution was prepared by dissolving the α,ω-bis-(propargyloxy)-PEG_{1000}/acrylated β-CD poly(pseudorotaxane) (2.8 g, 0.2 mmol) and 1-(3-azidopropyl)silatrane (0.13 g, 0.5 mmol) in anhydrous THF (40 mL). The latter reagent solution was subjected to repeated cycles of degassing under argon protection. The catalyst solution was added over the reagent mixture and similarly subjected to degassing under argon. The reaction mixture was stirred for 24 h at room temperature, followed by complete removal of the solvent under vacuum. The crude product was purified using flash chromatography on silica gel using a

7/3 mixture of methylene chloride/*n*-hexane, resulting in 2.5 g of a slight yellow white powder (85% yield).

^{1}H NMR (DMSO-d_6, 400.13 MHz, δ (ppm)): 0.16 (4H, s, CH_2–Si), 1.67–1.96 (4H, m, CH_2–CH_2–Si), 2.80 (12H, t, 5.2 Hz, CH_2–N), 3.46–3.73 (all –O–CH_2–CH_2–O– from PEG overlapped with H-4 from cyclodextrin), 3.61 (12H, bs, CH_2–O), 3.74–4.12 (H-3 and H-2 from cyclodextrin), 4.12–4.64 (H-5, H-6 and unreacted OH-6 from cyclodextrin), 4.80–5.32 (H-1 from cyclodextrin), 5.80–6.50 (OH-2, OH-3 from cyclodextrin and acrylic protons), 8.37 (2H, bs, CH-triazole).

Preparation of PEI decorated polyrotaxane (ROT-PEI). The synthesis of the vector based on the polyrotaxane decorated with PEI (Fig. S24†) was achieved by dissolving α,ω-bis-{1-[3-(silatranyl)prop-1-yl]-1*H*-1,2,3-triazol-5-yl}-PEG_{1000}/acrylated β-CD polyrotaxane (0.93 g, 0.07 mmol) in a chloroform/methanol (1 : 1 v/v) mixture (35 mL), followed by the addition of PEI (2 kDa) (5.26 g, 2.8 mmol). The reaction mixture was stirred at room temperature for 4 days. The solvents were removed and the crude product was dispersed in double-distilled water and subjected to dialysis in a 3500 MWCO cutoff dialysis membrane for 7 days against double distilled water. The final step consisted of freeze-drying the resulting product solution.

^{1}H NMR (D_2O, 400.13 MHz, δ (ppm)): 0.64 (bs, CH_2–Si), 2.5–4.0 (all the protons from PEI and cyclodextrin moieties), 3.71 (all the –O–CH_2–CH_2–O– from PEG), 5.08 (bs, H-1 from cyclodextrin), 8.07 (bs, CH-triazole).

Preparation of PEI and PEG_{750} decorated polyrotaxane (ROT-PEI-PEG_{750}). The synthesis of the vector based on the polyrotaxane decorated with PEI and short linear poly(ethylene glycol) (PEG_{750}) (Fig. S27†) was conducted in a 50 mL round bottom flask by dissolving α,ω-bis-{1-[3-(silatranyl)prop-1-yl]-1*H*-1,2,3-triazol-5-yl}-PEG_{1000}/acrylated β-CD polyrotaxane (0.54 g, 0.04 mmol) and methoxypoly(ethylene glycol)-amine hydrochloride (750 Da) (0.12 g, 0.16 mmol) in a chloroform/methanol (1 : 1 v/v) mixture (25 mL). The solution was stirred for 24 h at room temperature, after which PEI (2 kDa) (3.76 g, 2.0 mmol) was added and the reaction mixture was stirred for 4 days. The solvents were removed by vacuum distillation. The resulted crude product was dispersed in double-distilled water and subjected to dialysis in a 3500 MWCO cutoff dialysis membrane for 7 days against double distilled water. The final step consisted of freeze-drying of the resulting product solution.

^{1}H NMR (D_2O, 400.13 MHz, δ (ppm)): 0.60 (bs, CH_2–Si), 2.5–4.0 (all the protons from PEI and cyclodextrin moieties), 3.37 (OCH_3 groups from PEG), 3.71 (all the –O–CH_2–CH_2–O– from PEG), 5.05 (bs, H-1 from cyclodextrin), 8.05 (bs, CH-triazole).

Preparation of arginine decorated ROT-PEI (ROT-PEI-Arg). A previously reported protocol[76,77] was used to attach arginine residues on the superficial amino groups of the branched polyethyleneimine in the ROT-PEI (Fig. S30†). Briefly, one equivalent of ROT-PEI, twelve equivalents of Fmoc-Arg(pbf)-OH, HOBt, HBTU and 24 equivalents of DIPEA were dissolved in anhydrous DMF and stirred for 48 h at room temperature. In the next step, the reaction mixture was precipitated in a large excess of diethyl ether. The filtered solid product was dissolved in DMF and mixed with a 15% solution of piperidine in DMF in order to remove the Fmoc protecting groups. The removal of the 2,2,4,6,7-pentamethyldihydrobenzofuran-5-sulfonyl protecting group (pbf) was achieved with an acidic solution composed of TFA : TIPS : H_2O 95 : 2.5 : 2.5. The final product was subjected to dialysis against deionized water for 5 days in a 3.5 kDa cutoff Spectra/Por® membrane and subjected to freeze drying to remove the water.

^{1}H-NMR (D_2O, 400.13 MHz, δ (ppm)): 0.67 (bs, CH_2–Si), 1.60–1.80 (2 × CH_2 groups from arginine moieties), 2.5–4.0 (all the protons from PEI and cyclodextrin moieties), 3.22 (t, CH_2–NH from arginine moieties), 3.52 (t, CH groups from arginine moieties), 3.70 (all the –O–CH_2–CH_2–O– from PEG), 5.08 (bs, H-1 from cyclodextrin), 8.08 (bs, CH-triazole).

Preparation of guanidine decorated ROT-PEI (ROT-PEI-G). ROT-PEI-G was obtained by grafting guanidine on the superficial primary amino groups of ROT-PEI (Fig. S30†). In a typical experiment,[79] ROT-PEI (0.65 g, 0.0097 mmol) was dissolved in deionized water (20 ml) alongside 1*H*-pyrazole-1-carboxamidine hydrochloride (0.04 g, 0.27 mmol). The molar ratio between the two reaction components was 1 : 27 ROT-PEI : 1*H*-pyrazole-1-carboxamidine hydrochloride, in order to attach a guanidine addend to a single amino group in each branched PEI in the polyrotaxane structure. Following the complete dissolution of the two compounds, *N*,*N*-diisopropylethylamine (0.16 g, 1.23 mmol) (DIPEA) was added dropwise to the reaction mixture. The reaction mixture was stirred at room temperature for 72 h. In the next step, the excess amount of DIPEA was removed under vacuum distillation and the resulting solution was subjected to dialysis against deionized water for 5 days in a 3.5 kDa cutoff Spectra/Por® membrane. The solution was then freeze dried to remove the water.

^{1}H NMR (D_2O, 400.13 MHz, δ (ppm)): 0.62–0.66 (m, CH_2–Si), 2.30–4.00 (all the protons from PEI and cyclodextrin moieties), 3.66 (all the –O–CH_2–CH_2–O– from PEG), 5.02 (bs, H-1 from cyclodextrin), 8.03 (bs, CH-triazole).

Fourier transform infrared spectroscopy (FT-IR). The FT-IR spectra of the related compounds were recorded using a Bruker Vertex 70 FT-IR instrument, in transmission mode, at room temperature, with a resolution of 2 cm^{-1} and 32 scans. The samples were incorporated into dry KBr pellets.

NMR spectroscopy. NMR spectra were recorded on Bruker Avance DRX 400 and Bruker Avance III spectrometers, operating at 400.13 and 100.61 MHz for ^{1}H and ^{13}C nuclei, respectively, at room temperature. Due to the structural complexity of the analyzed compounds, several probes were used for the NMR analysis. Thus, all the 2D homo- and heteronuclear correlations were recorded using a 5 mm inverse detection, multinuclear, *z*-gradient probe. The ^{13}C-NMR spectra were recorded on either a 5 mm QNP (H, C, Si, F) direct detection, *z*-gradient probe or a 10 mm multinuclear, direct detection, *z*-gradient probe (the semi-quantitative ^{13}C experiment).

Signal assignments were made based on 2D NMR homo- and heteronuclear correlations like ^{1}H,^{1}H-COSY (Correlation Spectroscopy), ^{1}H,^{13}C-HSQC (Heteronuclear Single Quantum Coherence) and ^{1}H,^{13}C-HMBC (Heteronuclear Multiple Bond

Correlation) experiments, using standard pulse sequences in the version with *z*-gradients, as delivered by Bruker with TopSpin 2.1 PL6 spectrometer control and processing software. Chemical shifts are reported in ppm and referred to residual solvent peaks.

Elemental analysis. Determination of elemental compositions and compositional mapping of the samples have been performed using a scanning electron microscope Quanta 200 equipped with an energy-dispersive X-ray (EDAX) detector. X-ray intensities are measured by counting photons and the precision is limited by statistical error. Usually, for major elements a precision better than ±1% (relative) can be obtained.

Gel permeation chromatography. Weight-average molecular weights (M_w) and number-average molecular weights (M_n) were determined by means of a Polymer Laboratories gel permeation chromatograph equipped with a PL-EMD 950 Evaporative Mass Detector. The system was calibrated with polyethylene oxide standards within 22 680–298 000 Da molecular weight range. The standards were run through two in line PL Aquagel OH-40 Agilent columns (8 μm particle size) that were effective for separation of molecular weights from 10 000 to 200 000 Da. The molecular weight distribution was correlated with the retention time by a third-order calibration curve. Standards and samples with a concentration of 2 mg ml^{-1} were measured using aqueous NaN_3 (0.02%) as the eluent. The flow rate was maintained at 1 mL min^{-1} at t = 40 °C in the columns.

X-ray diffractograms. Wide Angle X-ray Diffraction (WAXD) patterns were recorded on a D8 Advance Diffractometer (Bruker AXS, Germany), using Cu-Kα radiation (λ = 0.1541 nm), a parallel beam with a Gobel mirror and a Dynamic Scintillation detector. The working conditions were 36 kV and 30 mA, count time: 2 s per step and step size: 0.02 degree per step. All diffractograms were investigated in the 2θ range of 4–50° at room temperature. Bruker "DIFFRAC-PLUS Evaluation – EVA" and "TOPAZ" software were used for data processing.

Agarose gel electrophoresis. Gel retardation assay was performed to electrophoretically evaluate the formation of the polyplexes, while unbound DNA molecules move through the gel separately toward the positive electrode after a specific migration profile, comparable to the control sample (DNA without vehicle). Both naked pGFP and the polyplexes obtained at different N/P ratios were mixed with loading buffer (1× TAE buffer, pH 7.4) and then loaded in a 1% agarose gel. Electrophoresis was carried out at 90 V, for 120 minutes, in TAE running buffer solution (40 mM Tris-HCl, 1% glacial acetic acid, 1 mM EDTA). The migration of free and complexed pGFP was visualized under UV light, after staining with ethidium bromide.

Size and zeta potential measurements of polyplexes. The size and zeta potential measurements were performed using a DelsaNano C Submicron Particle Size Analyser (Beckman Coulter), equipped with dual 30 mW laser diodes emitting at 658 nm. Measurements were performed at 25 °C, pH 7.4. The samples were prepared in PBS buffer, in a total volume of 3 mL. Each sample comprises the same amount of dsDNA (100 μg), varying the quantity of DNA vehicle, in order to achieve the desired N/P ratios. After an incubation time of 30 min, the polyplex solutions were loaded into the measuring cells.

Transmission electron microscopy (TEM). The size and morphology data of the cargo-complexes were obtained using a Hitachi HT7700 transmission electron microscope (TEM), operating at 100 kV, in high resolution mode. The polyplex samples were prepared as follows. 2 μl of each cargo-complex solution was deposited on carbon TEM grids (400 mesh) and was left for 24 hours to evaporate the solvent at room temperature, under atmospheric pressure, before examination.

Computational methods

Model construction. First, a model of randomly branched PEI (M_w = 2 kDa) was manually constructed using the Avogadro software.[23] The protonation states of the amino groups were manually adjusted to give an overall protonation of 50% on the entire molecule.[80] Then, a β-cyclodextrin was substituted with 3 PEI molecules at C6 carbon atoms, as obtained from synthesis. Nine tri-substituted cyclodextrin molecules were inserted on an extended PEG linear molecule (M_w = 1 kDa), and the silatrane stoppers were added at each end to build the polyrotaxane supramolecular aggregate. The complex was then solvated using Maestro simulation environment [Schrödinger, LLC, New York, NY, 2016] in a parallelepiped box with 49 582 water molecules, 786 Cl^- ions, and 138 Na^+ ions, to achieve system neutrality and a 150 mM salt concentration. The system was then energy minimized using the steepest descent algorithm.

Molecular dynamics (MD) simulations. The polyrotaxane aggregate was described using the OPLS-AA force field.[81] The TIP3P model was selected for water molecules. The constructed model was first subjected to equilibration, following Desmond molecular software standard relaxation protocol.[82] Production simulations were performed in the NPT ensemble at T = 300 K without any restraints applied on the system. The Nosé–Hoover chain method was used for thermostating (τ = 1.0 ps).[83,84] Martyna–Tobias–Klein (MTK) barostat was employed to isotropically keep the pressure constant at 1 atm (τ = 2.0 ps). Long range electrostatic interactions were evaluated using Particle-Mesh Ewald (PME) summation. Snapshots of the system configuration were saved every 1.2 ps for further analysis. Moments of inertia (MOI) and bi-dimensional particle number density charts were computed using the analysis utilities from the GROMACS molecular simulation package, after a prior conversion of the trajectories.[85] All simulations were performed using the parallel version of Desmond software on multiple processor equipped servers.

Evaluation of *in vitro* transfection efficiency

Preparation of plasmid DNA. Plasmids pCS2 + MT-Luc (pLUC) and pCS2 + NLS-eGFP (pGFP) (gift from Dr Adrian Salic, Harvard University, Boston) which encode for firefly luci-

ferase and enhanced green fluorescent protein, respectively, were grown in *E. coli* DH5α (gift from Dr Anca Gafencu, "Nicolae Simionescu" Institute of Cellular Biology and Pathology, Bucharest) and purified with E.Z.N.A. Endo-free Plasmid Mini II kit (Omega Bio-Tek, Inc.).

Preparation of cargo-complexes. The polyrotaxane samples were dissolved in pure water (Millipore), an appropriate amount of pDNA being then added and mixed by pipetting, followed by incubation at room temperature for 60 minutes before use.

Cell culture. HeLa (human cervix adenocarcinoma) cells from CLS-Cell-Lines-Services-GmbH (Germany) were maintained in complete medium: alpha-MEM medium (Lonza) supplemented with 10% fetal bovine serum (FBS, Gibco) and 1% penicillin–streptomycin–amphotericin B mixture (Lonza) in a 37 °C, 5% CO_2 humidified environment.

Transfection ability was determined as follows. Twenty four hours prior transfection, HeLa cells were plated at a density of 104 cells per well in 96-well white opaque microplates (PerkinElmer) and allowed to adhere overnight. The polyplexes were made by mixing pDNA with different concentrations of polymers in order to achieve desired N/P ratios for 500 ng DNA per well and were incubated at room temperature for one hour. After one hour, the transfection mixture was added to the cells without removing the medium. After 48 hours, the transfection efficiency was evaluated with a Bright-Glo™ Luciferase Assay System kit (Promega) on a plate reader (EnSight, PerkinElmer). Each experiment was performed in 8 replicates.

Cytotoxicity assay. Cytotoxicity was measured using the MTS technique (CellTiter 96® Aqueous One Solution Cell Proliferation Assay, Promega) which measures the mitochondrial reductase activity.[20,86] HeLa cells were seeded at a density of 104 cells per well in 96 well plates, in 100 μL complete medium. The next day, cells were transfected with polyplexes as described above, after which the cells were grown for another 44 hours. At least 8 biological replicates were performed for each polyplex type and N/P ratio, and each experiment was repeated 3 times. After 44 hours, 20 μL of CellTiter 96® Aqueous One Solution reagent were added to each well, and the plates were incubated for another 4 hours before reading the result. Absorbance at 490 nm was recorded with a plate reader (EnSight, PerkinElmer).

Conflicts of interest

There are no conflicts of interest to declare.

Acknowledgements

The authors are grateful for financial support from the H2020 WIDESPREAD 2-2014: ERA Chairs Project no. 667387: SupraChem Lab – Laboratory of Supramolecular Chemistry for Adaptive Delivery Systems, ERA Chair initiative.

Notes and references

1 S. L. Ginn, I. E. Alexander, M. L. Edelstein, M. R. Abedi and J. Wixon, *J. Gene Med.*, 2013, **15**(2), 65–67.
2 http://www.genetherapynet.com/clinical-trials.html (accessed March, 2017).
3 P. C. Bressloff and J. M. Newby, *Rev. Mod. Phys.*, 2013, **85**(1), 135–196.
4 A. Dinca, W.-M. Chien and M. T. Chin, *Int. J. Mol. Sci.*, 2016, **17**(2), 263.
5 Y. Kang, K. Guo, B.-J. Li and S. Zhang, *Chem. Commun.*, 2014, **50**, 11083–11092.
6 A. Siriviriyanun and T. Imae, in *Gene and Cell Therapy. Therapeutic Mechanisms and Strategies*, ed. N. Smyth Templeton, CRC Press, Boca Raton FL, USA, 4th edn, 2015, pp. 315–329.
7 G. Tavernier, O. Andries, J. Demeester, N. N. Sanders, S. C. De Smedt and J. Rejman, *J. Controlled Release*, 2011, **150**, 238–247.
8 A. S. Lewin and W. W. Hauswirth, *Trends Mol. Med.*, 2001, **7**(5), 221–228.
9 I. R. Graham and G. Dickson, *Biochim. Biophys. Acta, Mol. Basis Dis.*, 2002, **1587**(1), 1–6.
10 C. M. Uritu, M. Calin, S. S. Maier, C. Cojocaru, A. Nicolescu, D. Peptanariu, C. A. Constantinescu, D. Stan, M. Barboiu and M. Pinteala, *J. Mater. Chem. B*, 2015, **3**(42), 8250–8267.
11 J. A. Kretzmann, D. Ho, C. W. Evans, J. H. C. Plani-Lam, B. Garcia-Bloj, A. E. Mohamed, M. L. O'Mara, E. Ford, D. E. K. Tan, R. Lister, P. Blancafort, M. Norret and K. Swaminathan Iyer, *Chem. Sci.*, 2017, **8**, 2923–2930.
12 J. Jang, S. Ko and Y. Kim, *Adv. Funct. Mater.*, 2006, **16**, 754–759.
13 K. Wang, M. You, Y. Chen, D. Han, Z. Zhu, J. Huang, K. Williams, C. James Yang and W. Tan, *Angew. Chem., Int. Ed.*, 2011, **50**, 6098–6101.
14 Q. Yuan, Y. Wu, J. Wang, D. Lu, Z. Zhao, T. Liu, X. Zhang and W. Tan, *Angew. Chem., Int. Ed.*, 2013, **52**, 13965–13969.
15 M. R. Molla and P. A. Levkin, *Adv. Mater.*, 2016, **28**, 1159–1175.
16 M. Hanzlíková, M. Ruponen, E. Galli, A. Raasmaja, V. Aseyev, H. Tenhu, A. Urtti and M. Yliperttula, *J. Gene Med.*, 2011, **13**, 402–409.
17 Y. Yanan, *How Free Cationic Polymer Chains Promote Gene Transfection*, Springer International Publishing, Cham, Switzerland, 2013, pp. xv and 89.
18 C. M. Uritu, C. D. Varganici, L. Ursu, A. Coroaba, A. Nicolescu, A. I. Dascalu, D. Peptanariu, D. Stan, C. A. Constantinescu, V. Simion, M. Calin, S. S. Maier, M. Pinteala and M. Barboiu, *J. Mater. Chem. B*, 2015, **3**(12), 2433–2446.
19 L. Clima, D. Peptanariu, M. Pinteala, A. Salic and M. Barboiu, *Chem. Commun.*, 2015, **51**(99), 17529–17531.
20 I. A. Turin-Moleavin, F. Doroftei, A. Coroaba, D. Peptanariu, M. Pinteala, A. Salic and M. Barboiu, *Org. Biomol. Chem.*, 2015, **13**(34), 9005–9011.

21 F. M. Raymo and J. F. Stoddart, *Trends Polym. Sci.*, 1996, **4**, 208–211.
22 A. A. Travers, *Philos. Trans. R. Soc. London, Ser. A*, 2004, **362**, 1423–1438.
23 M. D. Hanwell, D. E. Curtis, D. C. Lonie, T. Vandermeersch, E. Zurek and G. R. Hutchison, *J. Cheminf.*, 2012, **4**, 1–17.
24 F. Ortega-Caballero, C. Ortiz Mellet, L. Le Gourriérec, N. Guilloteau, C. Di Giorgio, P. Vierling, J. Defaye and J. M. García Fernández, *Org. Lett.*, 2008, **10**(22), 5143–5146.
25 A. Díaz-Moscoso, L. Le Gourriérec, M. Gómez-García, J. M. Benito, P. Balbuena, F. Ortega-Caballero, N. Guilloteau, C. Di Giorgio, P. Vierling, J. Defaye, C. Ortiz Mellet and J. M. García Fernández, *Chem. – Eur. J.*, 2009, **15**, 12871–12888.
26 C. Aranda, K. Urbiola, A. Méndez Ardoy, J. M. García Fernández, C. Ortiz Mellet and C. Tros de Ilarduya, *Eur. J. Pharm. Biopharm.*, 2013, **85**, 390–397.
27 M. A. Islam, T.-E. Park, B. Singh, S. Maharjan, J. Firdous, M.-H. Cho, S.-K. Kange, C.-H. Yun, Y.-J. Choi and C.-S. Cho, *J. Controlled Release*, 2014, **193**, 74–89.
28 Q. Jiang, Y. Zhang, R. Zhuo and X. Jiang, *Colloids Surf., B*, 2016, **147**, 25–35.
29 J. A. Redondo, E. Martínez-Campos, L. Plet, M. Pérez-Perrino, R. Navarro, G. Corrales, A. Pandit, H. Reinecke, A. Gallardo, J. L. López-Lacomba, A. Fernández-Mayoralas and C. Elvira, *Macromol. Rapid Commun.*, 2016, **37**, 575–583.
30 F. Davis and S. Higson, *Macrocycles. Construction, Chemistry and Nanotechnology Applications*, John Wiley & Sons Ltd, Chichester, UK, 2011, ch. 9, p. 381–517.
31 J. Li, *J. Drug Delivery Sci. Technol.*, 2010, **20**(6), 399–405.
32 A. Harada and Y. Takashima, *Chem. Rec.*, 2013, **13**(5), 420–431.
33 K. Kato, K. Inoue, M. Kudo and K. Ito, *Beilstein J. Org. Chem.*, 2014, **10**, 2573–2579.
34 Y. Chen and Y. Liu, *Adv. Mater.*, 2015, **27**, 5403–5409.
35 J. Li, C. Yang, H. Li, X. Wang, S. H. Goh, J. L. Ding, D. Y. Wang and K. W. Leong, *Adv. Mater.*, 2006, **18**, 2969–2974.
36 T. Ooya, H. S. Choi, A. Yamashita, N. Yui, Y. Sugaya, A. Kano, A. Maruyama, H. Akita, R. Ito, K. Kogure and H. Harashima, *J. Am. Chem. Soc.*, 2006, **128**, 3852–3853.
37 J. J. Li, F. Zhao and J. Li, *Appl. Microbiol. Biotechnol.*, 2011, **90**, 427–443.
38 Y. Zhou, H. Wang, C. Wang, Y. Li, W. Lu, S. Chen, J. Luo, Y. Jiang and J. Chen, *Mol. Pharmaceutics*, 2012, **9**, 1067–1076.
39 Y. Yamada, M. Hashida, T. Nomura, H. Harashima, Y. Yamasaki, K. Kataoka, A. Yamashita, R. Katoono and N. Yui, *ChemPhysChem*, 2012, **13**, 1161–1165.
40 Q. Qin, X. Ma, X. Liao and B. Yang, *Mater. Sci. Eng., C*, 2017, **71**, 1028–1036.
41 N. Yui, *Macromol. Symp.*, 2009, **279**, 158–162.
42 J. E. Beves, B. A. Blight, C. J. Campbell, D. A. Leigh and R. T. McBurney, *Angew. Chem., Int. Ed.*, 2011, **50**, 9260–9327.
43 C. Gong and H. W. Gibson, in *Molecular Catenanes, Rotaxanes and Knots. A Journey Through the World of Molecular Topology*, ed. J.-P. Sauvage and C. Dietrich-Buchecker, Wiley-VCH Verlag GmbH, Weinheim, Federal Republic of Germany, 1999, pp. 277–321.
44 K. M. Wollyung, K. Xu, M. Cochran, A. M. Kasko, W. L. Mattice, C. Wesdemiotis and C. Pugh, *Macromolecules*, 2005, **38**, 257–2586.
45 P. Dandekar, R. Jain, M. Keil, B. Loretz, L. Muijs, M. Schneider, D. Auerbach, G. Jung, C.-M. Lehr and G. Wenz, *J. Controlled Release*, 2012, **164**(3), 387–393.
46 T. Higashi, K. Motoyama and H. Arima, *J. Drug Delivery Sci. Technol.*, 2013, **23**(6), 523–529.
47 M. Arunachalam and H. W. Gibson, *Prog. Polym. Sci.*, 2014, **39**, 1043–1073.
48 V. D. Badwaik, E. Aicart, Y. A. Mondjinou, M. A. Johnson, V. D. Bowman and D. H. Thompson, *Biomaterials*, 2016, **84**, 86–98.
49 A. Harada and M. Kamachi, *Macromolecules*, 1990, **23**, 2821–2823.
50 A. Harada, in *Synthesis of Polymers*, ed. A.-D. Schlüter, Wiley-VCH Verlag GmbH, Weinheim, Federal Republic of Germany, 1999, pp. 485–512.
51 Ph. A. Kalashnikov, V. I. Sokolov and I. N. Topchieva, *Russ. Chem. Bull. Int. Ed.*, 2005, **54**(8), 1973–1977.
52 S. Yamada, Y. Sanada, A. Tamura, N. Yui and K. Sakurai, *Polym. J.*, 2015, **47**, 464–467.
53 S. Chelli, M. Majdoub, G. Trippé-Allard, S. Aeiyach, K. I. Chane-Ching and M. Jouini, *Polymer*, 2007, **48**, 3612–3615.
54 M. J. Frampton and H. L. Anderson, *Angew. Chem., Int. Ed.*, 2007, **46**, 1028–1064.
55 J.-C. Olsen, K. E. Griffiths and J. F. Stoddart, in *From Non-Covalent Assemblies to Molecular Machines*, ed. J.-P. Sauvage and P. Gaspard, Wiley-VCH Verlag GmbH & Co., KGaA, Weinheim, Germany, 2011, pp. 67–139.
56 J. J. Michels, M. J. O'Connell, P. N. Taylor, J. S. Wilson, F. Cacialli and H. L. Anderson, *Chem. – Eur. J.*, 2003, **9**, 6167–6176.
57 L. Fang, M. A. Olson, D. Benítez, E. Tkatchouk, W. A. Goddard III and J. F. Stoddart, *Chem. Soc. Rev.*, 2010, **39**, 17–29.
58 V. Badwaik, Y. Mondjinou, A. Kulkarni, L. Liu, A. Demoret and D. H. Thompson, *Macromol. Biosci.*, 2016, **16**, 63–73.
59 T. Albuzat, M. Keil, J. Ellis, C. Alexander and G. Wenz, *J. Mater. Chem.*, 2012, **22**, 8558–8565.
60 A. Kulkarni, K. DeFrees, R. A. Schuldt, S.-H. Hyun, K. J. Wright, C. K. Yerneni, R. VerHeul and D. H. Thompson, *Mol. Pharmaceutics*, 2013, **10**(4), 1299–1305.
61 A. Kulkarni, K. DeFrees, R. A. Schuldt, A. Vlahu, R. VerHeul, S.-H. Hyun, W. Deng and D. H. Thompson, *Integr. Biol.*, 2013, **5**, 115–121.
62 A. Yamashita, D. Kanda, R. Katoono, N. Yui, T. Ooya, A. Maruyama, H. Akita, K. Kogure and H. Harashima, *J. Controlled Release*, 2008, **131**(2), 137–144.

63 V. Badwaik, L. Liu, D. Gunasekera, A. Kulkarni and D. H. Thompson, *Mol. Pharmaceutics*, 2016, **13**(3), 1176–1184.
64 Y. Yamada, T. Nomura, H. Harashima, A. Yamashita and N. Yui, *Biomaterials*, 2012, **33**, 3952–3958.
65 A. Yamashita, N. Yui, T. Ooya, A. Kano, A. Maruyama, H. Akita, K. Kogure and H. Harashima, *Nat. Protoc.*, 2006, **1**(6), 2861–1869.
66 A. Tamura and N. Yui, *J. Biol. Chem.*, 2015, **290**(15), 9442–9454.
67 J. J. Li, F. Zhao and J. Li, in *Biofunctionalization of Polymers and their Applications*, ed. G. S. Nyanhongo, W. Steiner and G. M. Gübitz, Springer-Verlag, Berlin, Germany, 2011, vol. 125, pp. 207–249.
68 T. Ooya and N. Yui, *J. Biomater. Sci., Polym. Ed.*, 1997, **8**(6), 437–455.
69 C. Wen, Y. Hu, C. Xu and F.-J. Xu, *Acta Biomater.*, 2016, **32**, 110–119.
70 J. K. Puri, R. Singh and V. Kaur Chahal, *Chem. Soc. Rev.*, 2011, **40**, 1791–1840.
71 M. G. Voronkov, *Bull. Acad. Sci. USSR, Div. Chem. Sci.*, 1991, **40**(12), 2319–2334.
72 M. G. Voronkov, V. M. Dyakov and S. V. Kirpichenko, *J. Organomet. Chem.*, 1982, **233**, 1–147.
73 S. Sok and M. S. Gordon, *Comput. Theor. Chem.*, 2012, **987**, 2–15.
74 M.-M. Fan, X. Zhang, J. Qin, B.-J. Li, X. Sun and S. Zhang, *Macromol. Rapid Commun.*, 2011, **32**, 1533–1538.
75 Y. Kang, X.-M. Zhang, S. Zhang, L.-S. Ding and B.-J. Li, *Polym. Chem.*, 2015, **6**, 2098–2107.
76 T. Kim, J. Baek, C. Z. Bai and J. Park, *Biomaterials*, 2007, **28**, 2061–2067.
77 S. Kim, J. H. Jeong, T. Kim, S. W. Kim and D. A. Bull, *Mol. Pharmaceutics*, 2009, **6**(3), 718–726.
78 T. Gensane, *Electron. J. Comb.*, 2004, **11**, R33.
79 T. Kim, M. Leeb and S. W. Kim, *Biomaterials*, 2010, **31**(7), 1798–1804.
80 C. Sun, T. Tang, H. Uluda and J. E. Cuervo, *Biophys. J.*, 2011, **100**, 2754–2763.
81 M. J. Robertson, J. Tirado-Rives and W. L. Jorgensen, *J. Chem. Theory Comput.*, 2015, **11**(7), 3499–3509.
82 K. J. Bowers, E. Chow, H. Xu, R. O. Dror, M. P. Eastwood, B. A. Gregersen, J. L. Klepeis, I. Kolossvary, M. A. Moraes, F. D. Sacerdoti, J. K. Salmon, Y. Shan and D. E. Shaw, Proceedings of the ACM/IEEE Conference on Supercomputing (SC06), Tampa, Florida, 2006.
83 G. J. Martyna, M. L. Klein and M. Tuckerman, *J. Chem. Phys.*, 1992, **97**, 2635–2643.
84 G. J. Martyna, D. J. Tobias and M. L. Klein, *J. Chem. Phys.*, 1994, **101**, 4177–4189.
85 M. J. Abraham, T. Murtola, R. Schulz, S. Páll, J. C. Smith, B. Hess and E. Lindahl, *SoftwareX*, 2015, vol. **1–2**, pp. 19–25.
86 J. A. Barltrop, T. C. Owen, A. H. Cory and J. G. Cory, *Bioorg. Med. Chem. Lett.*, 1991, **1**, 611–614.